Urbano-Bojorge, AL.; Casanova-Carvajal, O.; González, N.; Fernández, L.; Madurga, R.; Sánchez-Cabezas, S.; Aznar, E.... (2018). Influence of Medium Viscosity and Intracellular Environment on the Magnetization of Superparamagnetic Nanoparticles in Silk Fibroin Solutions and 3T3 Mouse Fibroblast Cell Cultures. Nanotechnology. 29(38):1-13. https://doi.org/10.1088/1361-6528/aacf4a

Influence of Medium Viscosity and Intracellular Environment on the Magnetization of Superparamagnetic Nanoparticles in Silkworm Fibroin Solutions and 3T3 Mouse Fibroblast Cell Cultures

Ana Lorena Urbano-Bojorge[1,2,a], Oscar Casanova-Carvajal[1,2,b], Nazario Félix-González[1,2,c], Laura Fernández[1,d], Rodrigo Madurga[1,2,e], Santiago Sánchez-Cabezas[3,f], Elena Aznar[2,3,g], Milagros Ramos[1,2,h] and José Javier Serrano-Olmedo[1,2,i*]

[1]Centro de Tecnología Biomédica (CTB), Universidad Politécnica de Madrid (UPM), Campus de Montegancedo, 28223, Pozuelo de Alarcón, Madrid, Spain.

[2]Centro de Investigación Biomédica en Red Bioingeniería, Biomateriales y Nanomedicina (CIBER-BBN), C/ Monforte de Lemos 3-5, Pabellón 11, 28029, Madrid, Spain

[3]Instituto Interuniversitario de Investigación de Reconocimiento Molecular y Desarrollo Tecnológico (IDM), Universitat Politècnica de València, València, Spain

[a]lorena.urbanob@upm.es, [b]oscar.casanova@ctb.upm.es, [c]nazario.felix@ctb.upm.es, [d]laura.fernandezg@ctb.upm.es, [e]rodrigo.madurga@ctb.upm.es, [f]santiago.sanchez@idm.upv.es, [g]elazgi@upvnet.upv.es, [h]milagros.ramos@ctb.upm.es and [i]josejavier.serrano@ctb.upm.es (corresponding author)

KEYWORDS: Superparamagnetic iron oxide nanoparticles (SPIONs), silkworm fibroin solutions, mouse 3T3 fibroblasts, alternating gradient magnetometer (AGM), fast field cycling NMR relaxometry (FFCNMR), viscosity.

ABSTRACT

Biomedical applications based on the magnetic properties of superparamagnetic iron oxide nanoparticles may be altered by the mechanical attachment or cellular uptake of these nanoparticles. When nanoparticles interact with living cells, nanoparticles are captured and internalized into intracellular compartments. Consequently, the magnetic behavior of the nanoparticles is modified.
In this paper, we investigated the change in the magnetic response of 14 nm magnetic nanoparticles (Fe_3O_4) in solutions, both as a stable liquid suspension (one of them mimicking the cellular cytoplasm) and when associated with cells. The field-dependent magnetization curves from inert fluids and cell cultures were determined by using a MicroMag™ 2900 Alternating Gradient Magnetometer (AGM system). The equipment was adapted to measure liquid samples because it was originally designed only for solids. In order to achieve this goal, custom sample holders were manufactured. Likewise, the Nuclear Magnetic Relaxation Dispersion (NMRD) profiles for the inert fluid were also measured by Fast Field Cycling NMR Relaxometry (FFCNMR). The results show that superparamagnetic iron oxide nanoparticles magnetization in inert fluids was affected by the carrier liquid viscosity and the concentration. In cell cultures, the mechanical attachment or confinement of superparamagnetic iron oxide nanoparticles inside cells accounted for the change in the dynamic magnetic behavior of the nanoparticles. Nevertheless, the magnetization value in cell cultures was slightly lower than that of the fluid simulating the viscosity of cytoplasm, suggesting that magnetization loss was not only due to

medium viscosity but also to a reduction in the mechanical degrees of freedom of superparamagnetic iron oxide nanoparticles rotation and translation inside cells.

The findings presented here provide information on the loss of magnetic properties when nanoparticles are suspended in viscous fluids or internalized in cells. This information could be exploited to improve biomedical applications based on magnetic properties as magnetic hyperthermia, contrast agents and drug delivery.

1. INTRODUCTION

In the last decade, the magnetic nanoparticles (MNPs) have been extensively used in a wide variety of applications in electronics [1], bioengineering [2], pharmacology [2, 3] and tissue engineering [4]. Nowadays, the most used iron oxide nanoparticles are magnetite (Fe_3O_4) and maghemite (Υ-Fe_2O_3) MNPs [5, 6]. Magnetite MNPs are mainly used in research and biomedical applications thanks to their biocompatibility [7]. Superparamagnetic Iron Oxide Nanoparticles (SPIONs) are particularly attractive in biomedical research [8]. Their magnetic properties allow nanoparticles to be manipulated by an external magnetic field [9] or excited by a time-varying magnetic field to generate heat [10, 11]. Furthermore, their small sizes comparable to cellular organisms (10-100 μm) allow for interactions with subcellular structures. These properties enable the MNPs to be used in applications as contrast agents (CA) [12], in drug delivery [13-14] and in generating magnetic hyperthermia [15-20], among others.

In magnetic hyperthermia, the conversion of electromagnetic energy into heat generated by SPIONs subjected to alternating magnetic fields (H_{AC}) can be used to cause tumor cell death [21, 22]. Recent studies have shown that the magnetic response, and hence the heating efficiency of SPIONs, is significantly reduced when these nanoparticles are placed in viscous carrier liquids [17, 23] and inside living cells or biological tissues [18, 24-30]. The greater viscosity of the biological environment and the spatial distribution or agglomeration of nanoparticles within intracellular organelles strongly influence the efficiency of SPIONs to increase the temperature of the surrounding medium [25-32]. These factors emerging from the nano-bio interaction make heating efficiency in *in vitro* applications less efficient and foreseeable than in ideal ferrofluids.

When MNPs are captured and internalized by macrophages, they accumulate in intracellular organelles like lysosomes [18, 29, 31-34], generating a decrease in the mechanical degrees of freedom in terms of MNP rotation and translation [15, 26, 35], which could affect their magnetic behavior. On the other hand, when MNPs are suspended in a viscous fluid, the viscosity of the medium and the nanoparticle concentration may generate a change in the magnetic moment relaxation processes of the MNPs [16, 23, 26, 36]. Precise knowledge about the distribution, fate and spatial localization of MNPs within a biological environment is still challenging. A better understanding the interactions of the cell-nanoparticle system is needed in order to control and optimize the magnetic properties of the MNPs for biomedical applications.

This work reports the change in the magnetic properties of 14 nm diameter SPIONs suspended in inert fluids: deionized water and solutions made of animal proteins such as silkworm fibroin at various viscosities, one of them comparable to the viscosity of cytoplasm [20]. Furthermore, the change in SPION nanomagnetism due to their mechanical attachment or confinement inside cells was analyzed and compared to the results obtained with the fibroin solution that simulated cytoplasm viscosity. This silkworm protein was used due to its promising properties in biomedical applications (drug delivery and regenerative neuroscience), as well as its biocompatibility and biodegradability [14, 37-38].

Saturation magnetization measurements, obtained from field-dependent hysteresis curves (M-H), were carried out in a MicroMag^{TM} 2900 alternating gradient magnetometer (AGM system) designed

by the Princeton Measurements Corporation, which was adapted to measure liquid samples. SMARTracer Fast Field Cycling NMR Relaxometry (FFCNMR), designed by Stelar, along with a Bruker electromagnet were used to measure the nuclear magnetic relaxation dispersion (NMRD) profiles of the magnetic colloids. The modified AGM system was used to determine the change in the magnetic behavior of SPIONs both suspended in a liquid medium and in contact with cells. It was found that the change in the magnetic properties of the SPIONs was influenced by the viscous medium, the biological environment and the SPION concentration.

2. MATERIALS AND METHODS

2.1. Superparamagnetic iron oxide nanoparticle synthesis

Superparamagnetic Iron Oxide Nanoparticles (SPIONs) were synthesized following a method described in the literature [39]. Iron (II) chloride tetrahydrate (498.0 mg, 2.50×10^{-3} mol) and iron (III) chloride hexahydrate (810.0 mg, 22.99×10^{-3}mol) were dissolved in a deoxygenated aqueous solution (600.0 mL, pH 1.5). Then, ammonium hydroxide aqueous solution (1.50 M) was added drop wise into the solution under vigorous stirring until the pH of the solution reached 9. The resulting black precipitate was isolated by centrifugation, washed with water until neutral pH, and then washed with ethanol. The final solid was dried under vacuum to obtain a Fe_3O_4 powder. The synthesized powder SPIONs were characterized using X-ray diffraction (XRD) and transmission electron microscopy (TEM). Representative images of the SPIONs showed well-defined nanoparticles with an average diameter of 14±3 nm. Typical reflections of iron oxide were observed in the powder XRD pattern in the range of $25° < 2\theta < 65°$. The corresponding Bragg peaks could be indexed with a cubic array of magnetite.XRD patterns were obtained on a Bruker D8 Advance diffractometer using CuKα radiation. TEM images were obtained with a JEOL JEM-1010 apparatus.

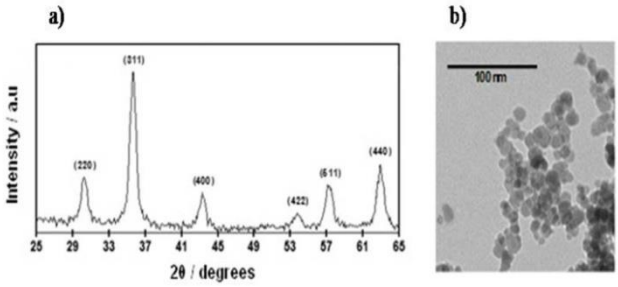

Figure 1. (a) Powder X-ray diffraction pattern; (b) Representative TEM image of synthesized SPIONs.

2.2. Silk fibroin synthesis

Silkworm cocoons (*Bombyxmori*) were degummed using a 0.2% (w/v) Na_2CO_3 solution. The ratio between the weight of silk cocoons and the Na_2CO_3 solution was 1/50 and the degumming process was performed at 121ºC for 50 minutes using an autoclave. The degummed silk was then rinsed and allowed to dry overnight. Once dried, the degummed silk was dissolved to a concentration of 10% (w/v) in a 9.4 M LiBr solution at 60ºC for 4 hours. This was followed by a dialysis step against deionized water using commercial Slide-A-Lyzer dialysis cassettes, with a molecular cut-off of 3.5 kDa, to remove the salts. Dialysis was performed for 3 days and the water was changed every 8 hours. The dialyzed fibroin solution was centrifuged (20 minutes at 5000 rpm) to remove any debris. Finally, the fibroin solution was frozen prior to lyophilization. The final product was a fibroin cake-like solid that could be dissolved to the desired concentration in water [40]. Liophilized silworm fibroin was

obtained as collaboration with Biomaterials and Regenerative Engineering Laboratory (CTB-UPM).

2.2.1 Silk fibroin phantom preparation

The lyophilized fibroin was weighed on a precision balance (Discovery SeriesDV215CDM from Ohaus). Afterward, small pieces of fibroin were added to a predetermined volume of deionized water while slow circular movements were performed to avoid the formation of surface scum in the sample. The solution was placed in a centrifuge (Rotina 380 from Hettich) at 5000 rpm and 24ºC for10 minutes to induce the decantation of non-dissolved pieces of fibroin. Finally, the fibroin solution was deposited into a new container and stored in the fridge at 8ºC. A total of three fibroin samples in which the viscosity was modified by changing the solute concentrations (0.062, 0.075 and 0.125 g/mL) were prepared. The viscosity values (η=3.31, η=4.12 and η=7.97mPa.s) were obtained at room temperature using a rotational viscometer (Alpha Series from Fungilab). It is worth noting that one of the viscosities (η=4.12mPa.s) was used as a phantom system that mimicked the biological-media viscosity of cytoplasm (η=4 mPa.s) [20].

2.2.2. Silk fibroin phantom with SPION samples

Using Eppendorf tubes, the SPIONs in powder were dispersed in fibroin solutions at three different concentrations (0.05, 2.5 and 10 mg/mL). In order to prevent physical changes in the fibroin samples associated with ultrasonic bath [38], these mixtures were shaken in a vortex mixer (Reax Control from Heidolph) for 20 minutes in order to obtain a stable colloid. Similarly, samples of a mixture of deionized water and SPIONs in powder were prepared, but an ultrasonic bath was used. It is important to highlight that silkworm fibroin was not used to coat the surface of SPIONs, but in order to perform suspensions with them.

2.2.3. Colloidal characterization and hydrodynamic size

Dynamic light scattering (DLS) is commonly used to determine the aggregation degree of MNPs in colloidal fluids by measuring hydrodynamic size (D_H). A Malvern Zetasizer Nano ZS was used to measure the D_H of synthesized SPIONs indeionized water and fibroin solution. Measurements were performed at 25ºC and the refractive indexes of magnetite and dispersant were set at 2 and 1.33, respectively.

2.2.4. Magnetization measurements

Magnetic characterization of SPIONs dispersed in deionized water and silk fibroin suspensions at three different viscosities and at the concentrations of 0.05, 2.5 and 10 mg/mL was carried out using the AGM. The probe of this equipment is built-in vertically, therefore homemade sample holders shaped like a well and made of colorless polymethyl methacrylate (PMMA) [41-42] (hereinafter referred to as sample holders$_{PMMA}$) were custom manufactured (Figure 2) to measure liquid samples.

The device was calibrated daily using standard reference material (SRM) 2853, i.e. a magnetic moment standard yttrium iron garnet sphere (YIG). Magnetization was assessed by measuring the hysteresis curves (M-H), setting the equipment to work in resonance mode due to its enhanced signal-to-noise ratio [43]. The measurements were carried out at room temperature, working with a maximum applied magnetic field from -1.2 to 1.2 Tesla.

Initially, the empty sample holder$_{PMMA}$ and the AGM probe were characterized to measure their diamagnetic response. Also, in order to characterize the magnetic colloid, the samples had to be shaken for 30 minutes to ensure a homogeneous colloid. A viscosity pipette (Transferpettor Dig. 10-50 µL from Brand) was used to extract ~14.5 µL of liquid sample, which was deposited into the sample holder and sealed with parafilm to prevent spillage. A thin layer of silicone grease (Dow Corning #112) was spread out on the AGM probe to hold the sample holder$_{PMMA}$. Finally, the probe and the sample holder containing the liquid sample were placed in the AGM for the characterization of the sample. These experiments were repeated at least five times.

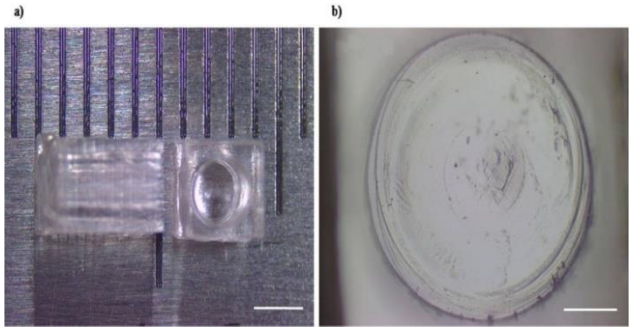

Figure 2. Image of the sample holder using a system Leica EZ4 W. (a) Side view (Scale bar = 2mm). (b) Bottom view (Scale bar = 0.5mm).

2.2.5. Relaxivity and NMRD profile measurements

The longitudinal relaxivity (r_1) of an aqueous fluid containing magnetic material in suspension, generally called contrast agent (CA), is defined as an increase in the longitudinal relaxation rate observed in aqueous solution when the concentration of the magnetically active compound is increased by one millimolar unit [12]. Relaxivities are generally defined by the slope of the linear regression generated from a plot of the measured relaxation rate (1/T) versus the concentration of the CA. The longitudinal relaxation is then calculated as follows:

$$1T1-1T1(0)=r1\cdot CA \quad (1)$$

where T1 denotes the longitudinal relaxation time of a solution containing CA, and T1(0) is the relaxation time of the solvent without CA; [CA] is the contrast agent concentration in mmol/L [44].

The longitudinal relaxation time (T1) measurements of SPIONs dispersed in water and silk fibroin phantoms at 2 mM concentration and at different viscosities were obtained on a FFCR apparatus from STELAR (SMARTracer) combined with a Bruker electromagnet of variable field strength ranging from 0.23 T up to 1.9 T. Using at least two different concentrations of SPIONs suspended in fluid samples allowed for the calculation of relaxivities at different field strengths. The dependency of relaxivity as a function of the magnetic field strength is known as the Nuclear Magnetic Relaxation Dispersion Profile (NMRD).

The measurements were performed at different magnetic field intensities (3 MHz, 5 MHz, 7 MHz, 9 MHz, 20 MHz and 40 MHz with a1H Larmor frequency). A saturation recovery (SR) sequence was employed to measure the T1 relaxation times, as specified by manufacturer. This sequence was performed by the digital NMR console of the SMARTracer, and consisted of a 90º pulse followed by a recovery time. A second 90º pulse was applied for refocusing and acquiring the Free Induction Decay (FID) curve.

Samples (150 µL for the Bruker electromagnet or 2 mL for the SMARTracer) at a magnetic colloid concentration of 2 mM, made as described above, were used in order to measure the longitudinal relaxation rates. Initially, the sample was deposited into RMN tubes with a long glass Pasteur pipette (Labolan #74770230, 230 mm). The water samples were sonicated for 10 minutes in an ultrasonicator,

while the fibroin samples were agitated in a vortex mixer for 15 minutes in order to homogenize the sample and suspend the SPIONs. The tube was finally placed inside of the probe coil of the Bruker electromagnet (high field) and the SMARTracer (low field). The relaxometry measurements were performed at 21°C.

2.3. Cell culture

The in vitro cytocompatibility of the sample holder$_{PMMA}$ was evaluated by culturing mouse fibroblasts (NIH/3T3; ATCC NCRL-1658). Sample holders$_{PMMA}$ were previously rinsed in double-distilled water and sterilized with ultraviolet light in a LabGard® Class II Biological Safety Cabinet for 20 minutes. Cells were cultured in Dulbecco's Modified Eagle's Medium (DMEM) supplemented with 5% heat-inactivated Fetal Bovine Serum (FBS), 2 mM L-glutamine, 0.1 mM of non-essential amino acids, 100 U/mL of penicillin, and 100 mg/mL of streptomycin (Life Technologies), hereinafter referred to as cell culture medium, and maintained in a humidified atmosphere at 37ºC with 5% CO_2 and 95% air.

2.3.1. Cell viability assays

In order to study the viability of cells cultured on the sample holders$_{PMMA}$, 3T3 cells were seeded at an initial density of $7.07x10^4$ cells/cm^2 and incubated for 24, 48 and 72 hours. Cell viability in the presence of SPIONs was also determined by incubating 3T3 cells in P24 multiwell plates at an initial density of $2.5x10^4$ cells/cm^2 with SPIONs at 1, 1.25, 2.5, 5 and 10 mg/mL for 24 hours. Two initial cell densities were tested since two different sample holders were going to be used. The sample holder of the AGM device (holder$_{PMMA}$) (Figure 2), where the cells were seeded at high density (7.07x104 cells/cm^2) to avoid cell-lacking areas in order to prevent nanoparticles from depositing at the bottom of the holder$_{PMMA}$. On the other hand, a standard multiwell plate (P24) with a cell density of 2.5x104 cells/cm^2 was used to observe the intracellular localization of the nanoparticles.

Cell viability was assessed using a calcein/PI (propidium iodide) dual-staining assay (Invitrogen/Molecular Probes). Cell culture medium was removed and cells were rinsed with phosphate-buffered saline (PBS; Gibco). Next, 1 μM calcein and 2 μM PI were added and incubated at 37°C for 20 minutes. Fluorescence was evaluated with an inverted Leica DMIRB microscope equipped with a Leica DC100 digital camera (Nussloch, Germany).

2.3.2. Intracellular localization of SPIONs

To determine the intracellular location of SPIONs, specific lysosome staining was used. 3T3 cells were seeded in P24 multiwell plates at a density of $2.5x10^4$ cells/cm^2 and incubated with 14 nm SPIONs at a concentration of 2.5 mg/mL for 24 hours. After incubation, cells were rinsed three times with PBS to eliminate excess nanoparticles and then incubated for 10 minutes with LysoTracker® Red DND-99 (Life Technologies) at 40 nM in cell culture medium. Analyses of fluorescent stained samples were carried out on a Leica DMIRB microscope equipped with a Leica DC100 digital camera (Nussloch, Germany).

2.3.3. Analysis of the magnetic behavior of SPIONs inside 3T3 cells

Once cell viability in the holder$_{PMMA}$ was verified, magnetization measurements were performed in order to assess the magnetic behavior of the SPIONs inside cells. For that purpose, 3T3 cells were

incubated with SPIONs at 2.5 mg/mL for 24 hours, and then cells were rinsed three times in PBS and analyzed in the AGM. To resuspend the internalized SPIONs, cells were rinsed in PBS, trypsinized for 10 minutes and sonicated for 5 minutes in an ultrasonic bath in order to liberate the magnetic material. The sample $holder_{PMMA}$ was measured once morein the AGM so as to compare the magnetic moment of the first and the second measurement (confined and unconfined SPIONs). Afterwards, the sample $holder_{PMMA}$ was rinsed to eliminate the SPIONs and dead cells. Once again, the $holder_{PMMA}$ was characterized in order to calculate the magnetization of the non-eliminated and adhered SPIONs to the $holder_{PMMA}$ walls. This value was adjusted in data processing. Finally, some sample $holders_{PMMA}$ from the same batch that had contained cells incubated with SPIONs were randomly selected to perform calcein/PI dual-staining assay in order to ascertain cell viability.

A calibration curve was carried out to calculate the approximate value of the SPION mass inside cells as from the magnetic moment measurements. For that purpose, a stock solution of SPIONs and trypsin-EDTA was prepared in order to imitate the condition of magnetic nanoparticles liberated from the cellular environment. Samples at several concentrations ranging from 0.05 mg/mL to 2.5 mg/mL were made from the stock solution. Next, the magnetic properties of these samples were measured in the AGM.

3. RESULTS AND DISCUSSION

3.1. Iron oxide nanoparticles

The structure, size and morphology of the synthesized nanoparticles were characterized. A typical XRD pattern (Figure 1(a)) indicates that the powder nanoparticles were monophasic with the inverse cubic spinel structure of Fe_3O_4 (magnetite). TEM images (Figure 1(b)) revealed that the nanoparticles were spherical and had a uniform size of about 14 nm. The diameter determined by TEM agrees with that calculated from the XRD pattern, indicating that the particles were highly crystalline. It is important to consider that, for biomedical applications, nanoparticles must have a size below 100 nm. Also, in order for these nanoparticles to be superparamagnetic, their size cannot exceed a few tens of nanometers [45].

3.2. Hydrodynamic size

The particle size distribution of the SPIONs dispersed in deionized water and fibroin solutions is shown in Figure 3. Particles suspended in deionized water presented a hydrodynamic size of ca. 40 nm, suggesting a slight aggregation tendency of SPIONs in water. This aggregation was increased in the presence of fibroin, to approximately 100 nm, which suggests that the increase in the size could be due to formation of SPION and fibroin aggregates. Thus, fibroin may be used as a surface coating agent due to its biocompatibility and easy internalization in living cells.

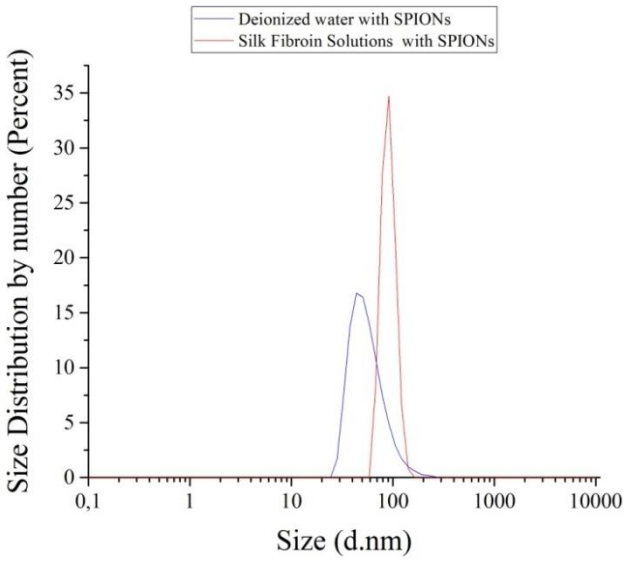

Figure 3. DSL measurements of magnetic colloids at 0.5 mg/mL.

3.3. Influence of the viscosity of the medium and concentration on the magnetism of SPIONs suspended in inert fluids

The magnetic moment values were normalized to the total SPION mass to obtain the magnetization (moments per unit mass), so that the curves are quantitatively comparable. Figure 4 shows the magnetization curves (M-H) as a function of the applied magnetic field for SPIONs dispersed in deionized water where they were able to move more freely (ideally free) and in fibroin solutions at several viscosities (ideally immobilized) and at concentrations of 2.5 and of 10 mg/mL. The experimental results showed a decrease in magnetization (M) in the magnetic colloid suspensions as the carrier fluid viscosity increased. This finding is in agreement with previous research [20, 23]. A magnetization value of dry SPIONs close to $65 Am^2/kg$ was reached beyond $H=\pm 8.0E^5$ A/m at room temperature. Zero remanence and coercivity corroborated the superparamagnetic behavior. Similar results of magnetization (64-70 emu/g_{magh}) have been published for iron oxide nanoparticles (7 up to 22 nm) in other studies using a vibrating sample magnetometer (VSM) [17].

At lower SPION concentrations, M values were similar independently of the dispersion media (Figure 4(a)). However, at higher concentrations, a clear distance between these values was observed (Figure 4(b)).

The shape of the magnetization slope varied according to the SPION concentration and the carrier liquid viscosity, becoming a bit stronger in fibroin solutions than in deionized water. The inclined magnetization slope might be due to the randomly orientated anisotropy axis with respect to the external field direction [17, 46-47]. SPIONs dispersed in fibroin solutions operate as small magnets with a randomly oriented anisotropic axis with respect to the external field direction or particle magnetization vector. As a consequence, the angle (θ) between the easy axis and magnetization vector is finite in the fibroin dispersions where SPIONs were quasi-immobilized. On the other hand, SPIONs dispersed in deionized water, where particles are free to rotate, favored alignment between the easy axis and magnetization vector ($\theta = 0$).

These results are in agreement with the classical theory that explains the magnetoviscous effect by the hindrance of free rotation of non-interacting single nanoparticles due to the magnetic torque that aligns the nanoparticle magnetic moments with the magnetic field direction [48, 49]. The magnetic interactions cooperate for the alignment between the easy axis and the nanoparticle magnetization vector when the SPIONs were immersed in low viscosity fluids. Conversely, easy axis alignment was

affected when particles were quasi-immobilized in high viscosity fluids (fibroin solution at η=7.97mPa.s).It is also well-known that, as the magnetic field intensity increases, the magnetic field can bring about aggregation and formation of chain-like structures, which lead to an increase in the viscosity of the magnetic colloid and hence a loss of magnetization [50, 51].

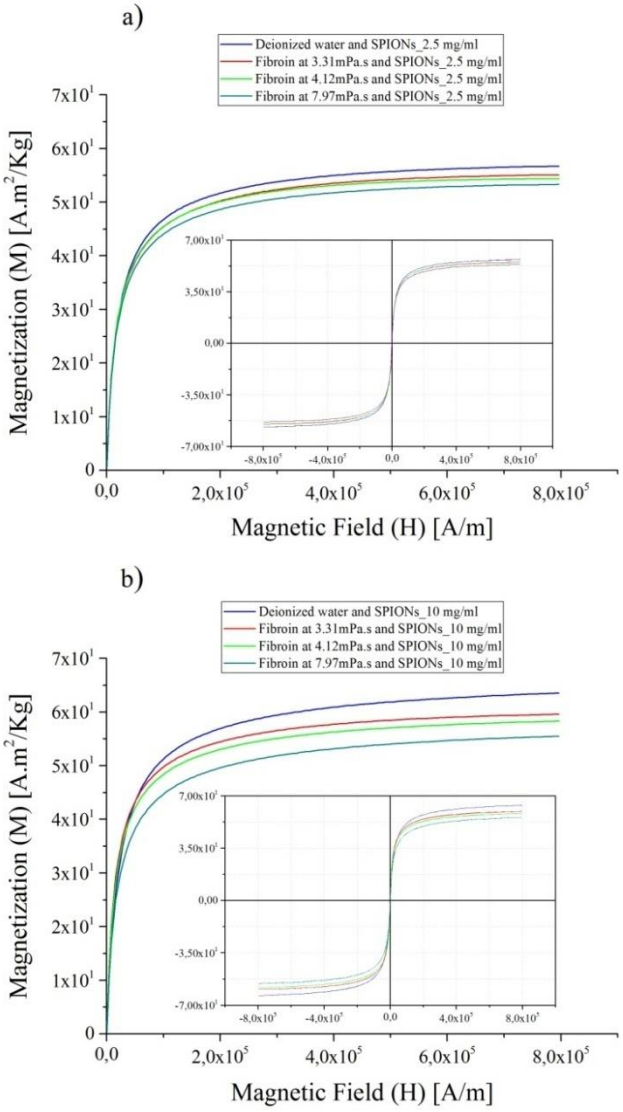

Figure 4. SPION mass-normalized magnetization curves as a function of the applied magnetic field and viscosity at (a) 2.5 mg/mL and (b) 10 mg/mL.

An increase in the nanoparticle concentration favored magnetic dipolar interactions, which led to a significant modification of magnetic relaxation, magnetization and heat dissipation. The presence of interactions between the MNPs is suggested by the normalized magnetization curves [52].

Figure 5 shows the magnetization curves normalized to M/M_s, where M and M_s are the magnetization and saturation magnetization of the system. In the weak magnetic field region, the slope of the magnetization curve was steeper for suspended SPIONs than for SPIONs in powder form or in highly concentrated fluids. This fact suggests that, as the nanoparticle concentration increases, the alignment of nanoparticle magnetic moments along the external magnetic field is hindered due to the short distance between the particles.

Figure 5(a) shows the dipolar interactions of SPIONs suspended in deionized water at 2.5 mg/mL, 10 mg/mL and powdered MNPs. The slope of the magnetization curve was steeper for the sample at

2.5 mg/mL than for the sample at 10 mg/mL but, at the same time, steeper than that of powdered nanoparticles. This same behavior has been observed in colloids with MNPs of similar sizes.

Figure 5(b) characterizes the dipole-dipole interactions of SPIONs suspended in deionized water or fibroin solutions (three different viscosities) at 2.5 mg/mL and SPIONs in powder. As can be observed, the magnetization curve of the liquid samples does not significantly differ with the media viscous and is steeper than for powder nanoparticles. This result indicates that the dipolar interactions within the nanoparticle system at 2.5 mg/mL do not exist or are smaller than the magnetic interactions in more concentrated liquid samples (10 mg/mL) or a nanoparticle system in the solid state. These findings are in agreement with those published in the literature [17, 53-55].

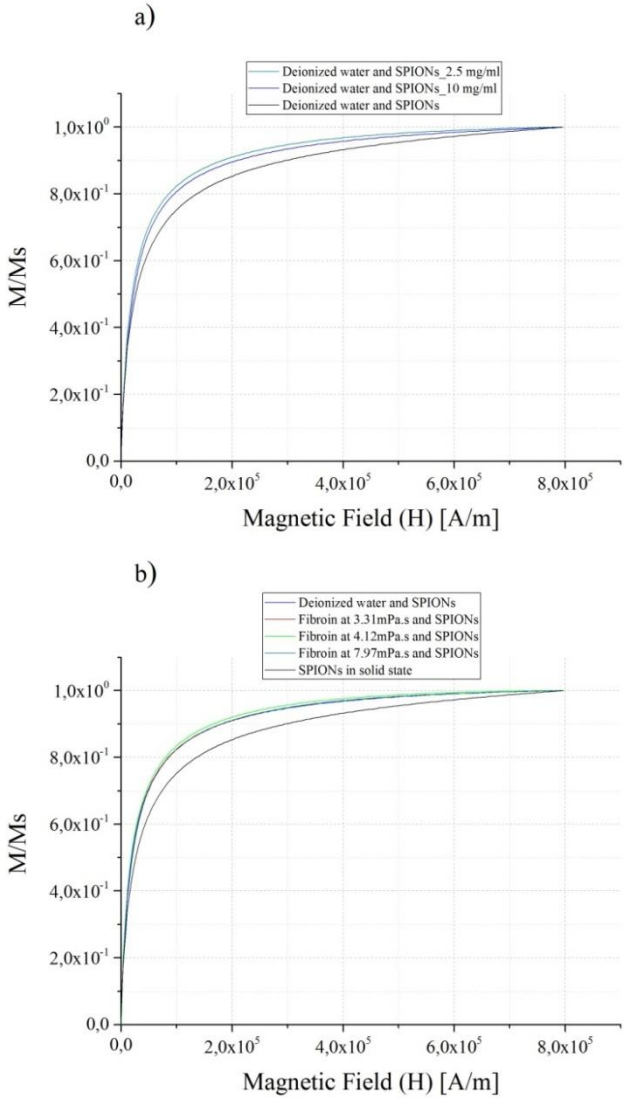

Figure 5. Normalized magnetization curves (M/M_s vs H) for a) SPIONs suspended in deionized water (2.5 and 10 mg/mL) and powdered SPIONs and b) SPIONs suspended in deionized water and fibroin at 2.5 mg/mL and powdered SPIONs.

3.4. Impactof viscosity on the relaxivity (r_1) of SPIONs dispersed in inert fluids

Figure 6 shows the relaxivity (r_1) as a function of the Larmor frequency in colloidal suspensions of SPIONs at 2 mM. At a low magnetic field strength, an increase in relaxivity was induced by the viscosity of the carrier liquid, which increased the rotational correlation time and induced high

relaxivity [56]. Conversely, the increase in r_1 was negligible at low viscosities. The fact that the relaxation rate was lower in water and in low viscosity solutions than in higher viscosity solutions indicates a high accessibility of water molecules to the surface of the SPIONs. Conversely, with high sample viscosities, the surface of the SPIONs was, in part, shielded from free water by the fibroin matrix. This process implies that the accessibility of free water to the surface of SPIONs is the origin of the dependence of r_1 values on the sample fluid viscosity, as samples with high viscosity have higher values of r_1.

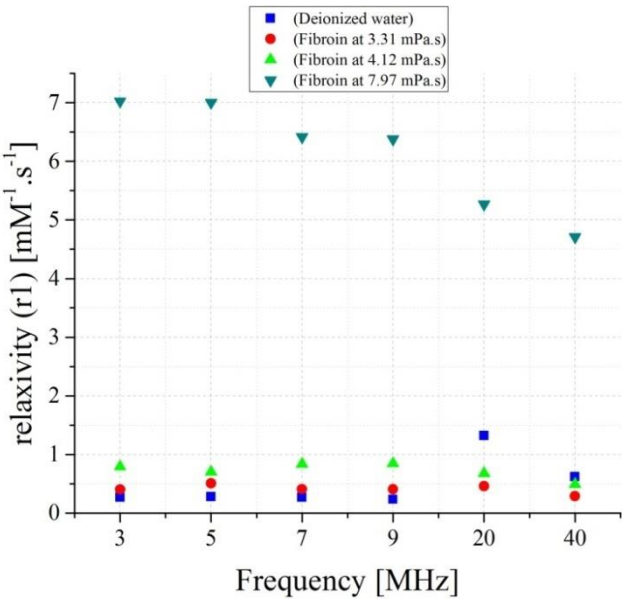

Figure 6. Nuclear magnetic relaxation dispersion profile (NMRD) at a colloid concentration of 2 mM.

3.5. Influence of SPION internalization by 3T3 cells on their magnetic behavior

3.5.1. Cell viability in sample holders fabricated from polymethyl methacrylate (PMMA) for AGM

In order to assess the efficiency of the sample holders$_{PMMA}$ to guarantee cell growth, the viability of 3T3 cells growing on PMMA and standard polystyrene wells was determined after 24, 48 and 72 hours of incubation. The results shown in Figure 7 indicate that sample holders$_{PMMA}$ did not significantly affect 3T3 cell viability, as evaluated by the calcein/PI assay. These results suggest that the sample holders$_{PMMA}$ did not induce acute cell toxicity at the time points analyzed. The slight decrease in cell viability was observed in sample holders$_{PMMA}$ after 72 hours of incubation, possibly due to the spatial limitation of the surface of the sample holders$_{PMMA}$, which may have prevented cell proliferation during the time period studied.

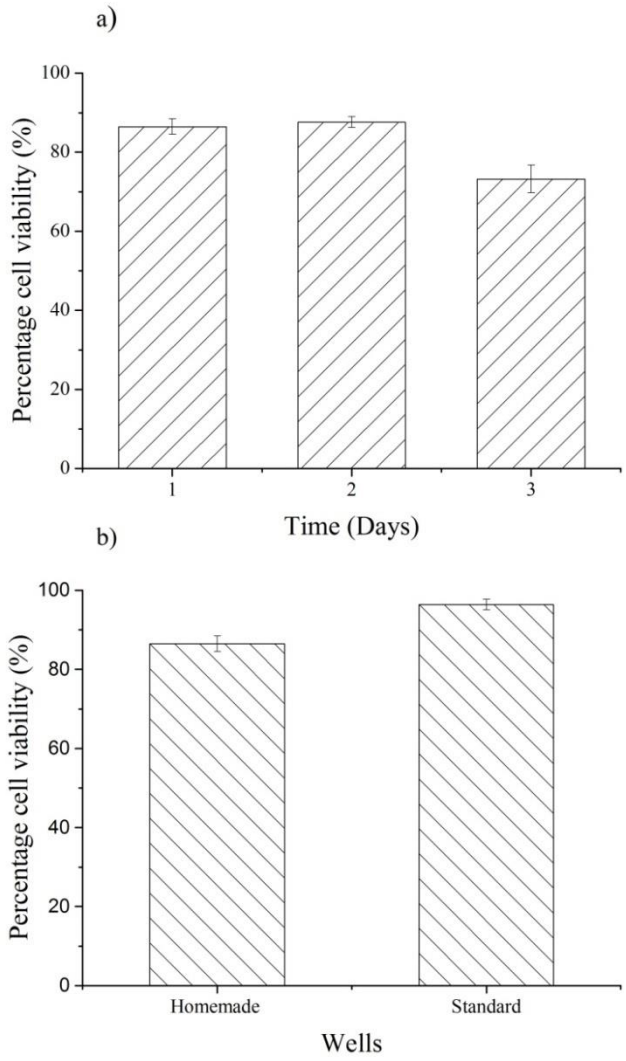

Figure 7. (a) Viability of 3T3 cells seeded on PMMA and (b) conventional polystyrene plates (standard) after 24, 36 and 72 hours of incubation. Cell viability was evaluated by the calcein/PI dual-staining assay. Data represent the mean ± SEM (standard error of the mean) of three independent experiments. ANOVA followed by the Tukey post hoc test revealed the absence of significant differences ($p<0.05$) for each group compared to cells seeded in standard wells.

3.5.2. Cell viability after incubation with SPION

Cell viability at high SPION concentrations, 5 and 10 mg/ml, was too low (Table 1). However, using lower concentrations (ranging from 1 mg/ml to 2.5 mg/ml) no statistically significant differences in cell viability between control and SPION-treated cells were found. Therefore, we chose the highest concentration of this last group to perform at least three independent experiments. Regarding the localization of SPION inside the cells, it is unfeasible to use a concentration of 10 mg/ml, since the cell viability is very low (see table 1). A SPION concentration of 2.5 mg/ml was considered the maximum concentration that keeps an optimal cell viability, and high enough to determine the final location of the phagocytized nanoparticles.

Table 2. Percent cell viability for different SPION concentrations at 24 hours. Data represent the mean ± SEM (standard error of the mean) of three independent experiments.

Sample concentration (mg/ml)	Percentage cell viability (%)
Control	99.28 ± 0.33
1	93.03 ± 0.79
1.25	90.38 ± 2.37
2.5	88.57 ± 0.85
5	60.22 ± 11.18
10	2.51 ± 0.14

The incubation of 3T3 cells with SPIONs was feasible and did not impair cell viability *in vitro*. 3T3 cells were incubated with SPIONs and tested for viability using doses up to 2.5 mg/mL for 24 hours, which did not significantly affect 3T3 cell survival, as evaluated by the calcein/PI assay (Figure 8). These results suggest that the levels of intracellular iron accumulation resulting from the incubation with SPIONs did not induce acute cell toxicity at the times and concentrations analyzed. These results are in accordance with previous reports showing that iron oxide nanoparticles are biocompatible with 3T3 cell cultures [57, 58].

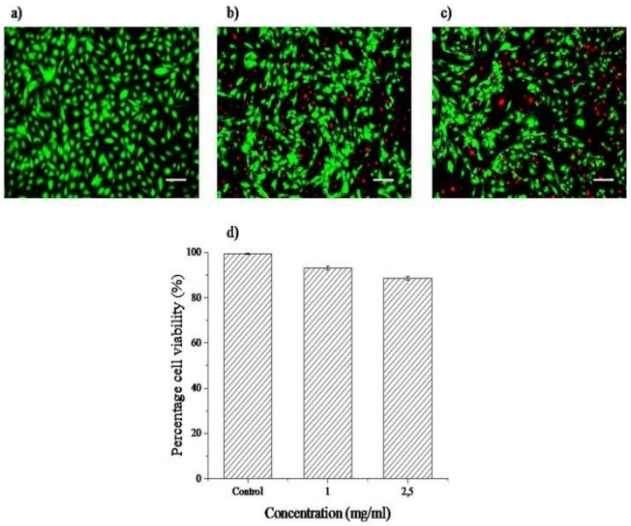

Figure 8. Viability of 3T3 cells incubated with SPIONs. Cells were incubated with SPIONs at 0 (a), 1 (b) and 2.5 (c) mg/mL for 24 hours and stained with calcein and propidium iodide to visualize live (green) and dead (red) cells, respectively. Data shown in (d) represent the quantification of the cell viability for each condition. Data represent the mean ± SEM of three independent experiments. ANOVA followed by the Tukey post hoc test revealed the absence of significant differences ($p<0.05$) for each group compared to control cells seeded without SPIONs (Scale bar = 50 μm).

3.5.3. Intracellular localization of SPIONs

To determine the final intracellular localization of the SPIONs, a fluorescent marker specific for lysosomes was used. When 3T3 cells were incubated with SPIONs for 24 hours, most of the particles were internalized by the cells and accumulated in intracellular vesicles, specifically in lysosomes, as determined by microfluorescence. In the Figure 9, the presence of SPIONs, visualized under light transmission as black spots (Figure 9(a)), showed strong co-localization with the fluorescent lysosome

marker (Figure 9(b)), indicating that most of the SPIONs were stored in the cells inside these organelles.

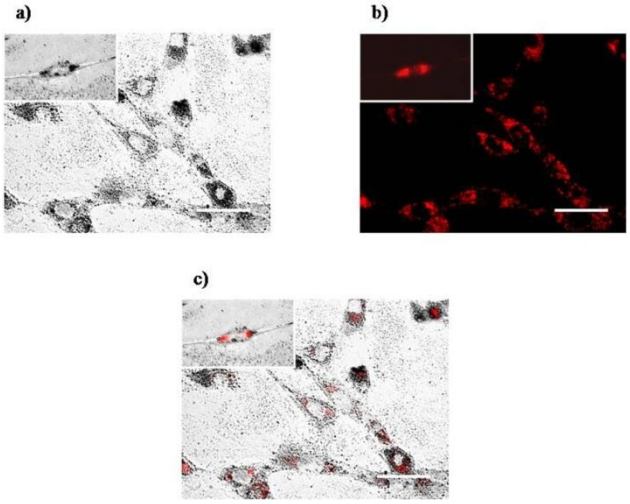

Figure 9. Intracellular location of SPIONs in 3T3 cells. 3T3 cells were incubated with SPIONs at a concentration of 2.5 mg/mL for 24 hours. SPIONs are shown by light transmission microscopy (a). Cells were stained with a specific marker for lysosomes in red (b). The localization of SPIONs and lysosomes can be visualized (c). (Scale bar = 50 μm).

3.5.4. Magnetic behavior measurements and method for determining the estimated amount of SPIONs internalized into 3T3 cells

To verify that SPIONs internalized into cells induce changes in their magnetic behavior, magnetization curves (M-H) were obtained for SPIONs in free suspension and following cellular interaction. Figure 10 shows the magnetic behavior of SPIONs inside 3T3 cells and SPIONs in free suspension, released when cells were sonicated. A decrease in the M value was observed when the SPIONs were inside cells compared to the M value obtained when the same SPIONs were in free suspension after being released from cells. The decrease in the M value indicated that the magnetic response of the particles was altered after cellular interaction with a reduction of around 14 Am^2/kg.

After measurements with the AGM, cell death was evaluated by the calcein/PI assay. The cell viability when SPIONs incubated in 3T3 cells were left outside the incubator for 30 (86.74%) and 60 minutes (84.51%) did not significantly affect cell viability at the time points analyzed. Each measurement was carried out for 1 hour.

In order to determine the shift in the magnetic response of the SPIONs in free suspension depending on their concentration, the magnetic moment of increasing concentrations of SPIONs ranging from 0.05 mg/mL to 2.5 mg/mL was determined (Figure 11). These data allowed us to quantify the amount of SPIONs present inside the cells since the SPIONs were released after the incubation period. Likewise, the magnetization of the SPIONs in these two cases was determined.

It is noteworthy that the concentration of 0.05 mg/ml corresponds to an experimental result of the calibration curve when the nanoparticles were internalized in the cells.

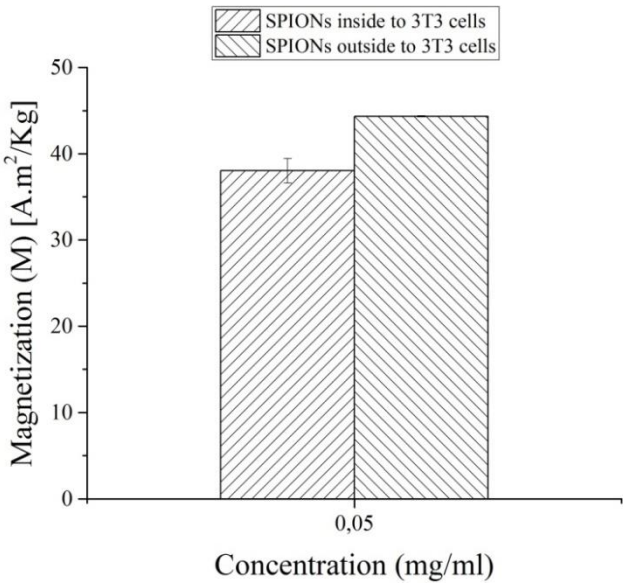

Figure 10. The magnetization values of SPIONs inside cells and those released from them.

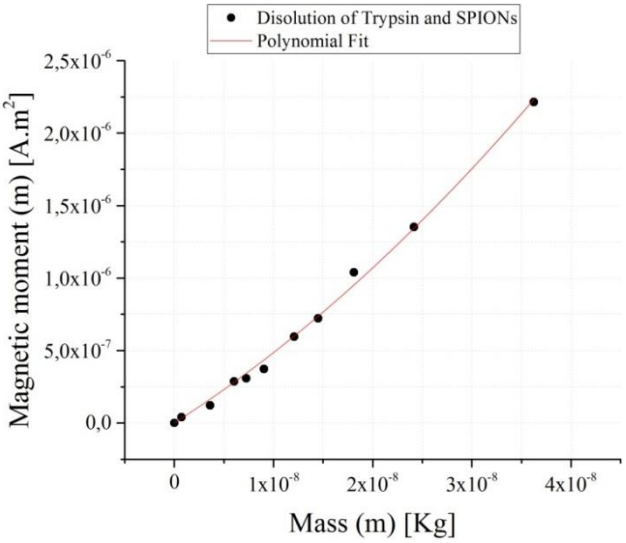

Figure 11. Calibration curve for a suspension of SPIONs and trypsin-EDTA at different concentrations.

It is well-known that when MNPs are taken up by cells through the endocytic route [59], these nanoparticles invaginate into vesicles (early endosomes), forming large aggregates [32, 33]. These vesicles subsequently fuse with intracellular organelles (late endosomes and lysosomes). During this process, MNPs encounter compartments with continuously decreasing pH and enzymatic activity. Finally, the MNP send up in lysosomes where they undergo degradation [28]. As a consequence, the magnetic properties of MNPs are modified during these processes. Increase in the local concentration of MNPs by cellular clustering prevents nanoparticles from behaving as isolated particles. Therefore, each of these particles experience dipolar interactions with their adjacent particles, which significantly change their dynamic magnetic behavior [60]. The experimental results of the present study indicated that SPIONs had lost their original magnetic properties and they seemed to be related to dipolar interactions, which might be favored by the intracellular formation of nanoparticle aggregates [27, 29] or due to the switch of nature of the magnetic moment relaxation processes induced by the increase in viscosity [26, 36].

According to the calibration curve, the cellular uptake of iron was estimated as 145 pg per cell after incubating 3T3 cells with SPIONs at 2.5 mg/mL for 24 hours. Table 2 shows that the M value of

SPIONs inside cells was slightly lower than in the fibroin solution that emulated the viscosity a biological medium (cytoplasm; η≈4 mPa.s). This result suggests that the reduction is not due to the carrier liquid viscosity but to the internalization of SPIONs incellular organelles (lysosomes) which generates large aggregates of SPIONs. Hence, the Brownian relaxation was affected by the reduced mobility of particle magnetic moments. Conversely, the M of SPIONs in the fibroin solution was a little higher because the SPION magnetic moments followed the alignment of the magnetization vector.

Table 2. Comparison of magnetization values of SPIONs in fibroin viscous fluid (η=3.31, 4.12 and 7.97 mPa.s) and in 3T3 mouse fibroblasts. Data represent the mean ± SEM (standard error of the mean).

Sample	**Magnetization (M) [Am^2/kg]**		
	Concentration 0.05 mg/mL	**Concentration 2.5 mg/mL**	**Concentration 10 mg/mL**
Fibroinη=3.31mPa.s and SPIONs	40.60±0.45	55.22±0.13	59.60±0.19
Fibroin η=4.12mPa.s and SPIONs	**39.20±0.42**	54.44±0.10	58.35±0.11
Fibroin η=7.97mPa.s and SPIONs	36.86±0.50	53.50±0.24	55.36±0.24
3T3 cells with internalized SPIONs	**38.01±1.44**	-	-
3T3 cells with non-internalized SPIONs	43.92±0.07	-	-

4. CONCLUSIONS

Magnetometry measurements of SPIONs with a mean diameter of 14 nm suspended in deionized water, silk fibroin solutions at different viscosities and 3T3 mouse fibroblasts were carried out to determine the influence of viscosity and the intracellular environment on their magnetism. In inert fluids, the magnetic properties of the SPIONs were altered by the viscous media, the formation of aggregates and the magnetoviscous effect. In cell cultures, the change in the magnetic properties of SPIONs may have been due to mechanical adhesion to cell membranes and subsequent internalization, which led to a decrease of in mechanical degrees of freedom of SPION rotation and translation. In this way, nanomagnetism might provide evidence of the localization of SPIONs in cells. All the results conclude that most of the nanoparticles always accumulate intracellularly in lysosomes at all the different times and concentrations tested (see figure 9), indicating that the internalized magnetic content has a minimal or null influences on the cellular uptake pathway. On the other hand, the results show that the magnetization measurements of SPIONs in fibroin solution at η=4.12 mPa.s were an indirect measure of the real viscosity of the cytoplasm, which has been studied in the literature. The adaptation of the non-industrial manufacturing sample holder to be used in AGM was validated to measure the magnetic response of SPIONs in liquid samples and living cells. Moreover, the r1 and M measurements of magnetic colloids were correlated with viscosity, showing an increase and decrease, respectively, when the carrier fluid viscosity was increased. With regard to r1, this characteristic is considered highly important for the design of a contrast agent that could be encapsulated in fibroin molecules to reduce the SPION concentration and hence the toxicity.

ACKNOWLEDGMENTS

The authors would like to thank Francisco Mikuski and Soledad Martinez from the Centre for Biomedical Technology (CTB) for manufacturing the holder samples that were used in the AGM and for cell culture training, respectively. The authors would also like to show gratitude to Edgar Pérez Esteve of the Food Technology Department of the Technical University of Valencia for the DLS measurements. The authors also thank PhD. Teresa López de Mora for critical review of the manuscript.

The authors are thankful to their supporters: a grant from the Technical University of Madrid to Ana Lorena Urbano-Bojorge and a grant from Universidad Nacional Experimental del Táchira (UNET)– Venezuela to Oscar Casanova-Carvajal. This study was also financially supported in part by CIBER-BBN (Spain) and Madr.ib-CM (Spain).

The characterization of MNPs was performed at the ICTS NANBIOSIS, Unit 15 (*Functional Characterization of Magnetic Nanoparticles*) of the CIBER in Bioengineering, Biomaterials &Nanomedicne (CIBER-BBN) at the Center for Biomedical Technology (CTB) of the Technical University of Madrid (UPM).

CONFLICT OF INTEREST:

No conflict of interest was reported by the authors of this paper.

REFERENCES

1. Ko S H, Park I, Pan H, Grigoropoulos C P, Pisano A P, Luscombe CK, Fréchet J M 2007 Direct nanoimprinting of metal nanoparticles for nanoscale electronics fabrication *Nano letters* **7**1869-1877.
2. Ilkhani H, Hughes T, Li J, Zhong C J, Hepel M 2016 Nanostructured SERS-electrochemical biosensors for testing of anticancer drug interactions with DNA *Biosensors and Bioelectronics* **80**:257-264.
3. Zaloga J, Pöttler M, Leitinger G, Friedrich R P, Almer G, Lyer S, Dörje F 2016 Pharmaceutical formulation of HSA hybrid coated iron oxide nanoparticles for magnetic drug targeting. *European Journal of Pharmaceutics and Biopharmaceutics* **101**152-162.
4. Bañobre-López M, Piñeiro-Redondo Y, De Santis R, Gloria A, Ambrosio L, Tampieri A, Dediu V, Rivas J 2011 Poly(caprolactone) based magnetic scaffolds for bone tissue engineering *J. Appl. Phys.* **109**: 07B313.
5. Gupta A K, Gupta M 2005 Synthesis and surface engineering of iron oxide nanoparticles for biomedical applications *Biomaterials* **26** 3995-4021.
6. Soares P I, Alves A M, Pereira L C, Coutinho J T, Ferreira I M, Novo C M, Borges J P 2014 Effects of surfactants on the magnetic properties of iron oxide colloids *Journal of colloid and interface science* **419** 46-51.
7. Cheng F Y, Su C H, Yang Y S, Yeh C S, Tsai C Y, Wu C L, Shieh D B 2005 Characterization of aqueous dispersions of Fe3O4 nanoparticles and their biomedical applications *Biomaterials* **26** 729-738.
8. Hilger I, Kaiser W A 2012 Iron oxide-based nanostructures for MRI and magnetic hyperthermia *Nanomedicine* **7** 1443-1459.
9. Leslie-Pelecky D L, Rieke R D 1996 Magnetic properties of nanostructured materials *Chemistry of materials* **8** 1770-1783.
10. Pankhurst Q A, Connolly J, Jones S K, Dobson J J 2003 Applications of magnetic nanoparticles in biomedicine *Journal of physics D: Applied physics* **36** R167.
11. Lu A H, Salabas E E, Schüth F 2007 Magnetic nanoparticles: synthesis, protection,

functionalization, and application *Angewandte Chemie International Edition* **46** 1222-1244.
12. Félix‐González N, Urbano‐Bojorge A L, Mina‐Rosales A, Pozo‐Guerrero F, Serrano‐Olmedo J J 2016 Assessment of a Heuristic Model for Characterization of Magnetic Nanoparticles as Contrast Agent in MRI *Concepts in Magnetic Resonance Part A* **44A** 279-286.
13. Majeed M I., Lu Q, Yan W, Li Z, Hussain I., Tahir M N, Tan B 2013 Highly water-soluble magnetic iron oxide (Fe_3O_4) nanoparticles for drug delivery: enhanced in vitro therapeutic efficacy of doxorubicin and MION conjugates *Journal of Materials Chemistry B* **1** 2874-2884.
14. Chen A Z, Chen L Q, Wang S B, Wang Y Q, Zha J Z 2015 Study of magnetic silk fibroin nanoparticles for massage-like transdermal drug delivery *International journal of nanomedicine* **10** 4639-4651.
15. Piñeiro Y, Vargas-Osorio Z, Bañobre-López M, Kolen'ko Y V, López-Quintela M A, Rivas J 2016 Relevant Parameters for Magnetic Hyperthermia in Biological Applications: Agglomeration, Concentration, and Viscosity *IEEE Transactions on Magnetics* **52** 1-4.
16. Ovejero J G, Cabrera D, Carrey J, Valdivielso T, Salas G, Teran F J 2016 Effects of inter-and intra-aggregate magnetic dipolar interactions on the magnetic heating efficiency of iron oxide nanoparticles *Physical Chemistry Chemical Physics* **18** 10954-10963.
17. Salas G, Camarero J, Cabrera D, Takacs H, Varela M, Ludwig R, Teran F J 2014 Modulation of magnetic heating via dipolar magnetic interactions in monodisperse and crystalline iron oxide nanoparticles *The Journal of Physical Chemistry C* **118** 19985-19994.
18. Di Corato R, Espinosa A, Lartigue L, Tharaud M, Chat S, Pellegrino T, Wilhelm C 2014 Magnetic hyperthermia efficiency in the cellular environment for different nanoparticle designs *Biomaterials* **35** 6400-6411.
19. Serantes D, Simeonidis K, Angelakeris M, Chubykalo-Fesenko O, Marciello M, Morales M D P, Martinez-Boubeta C 2014 Multiplying magnetic hyperthermia response by nanoparticle assembling *The Journal of Physical Chemistry C* **118** 5927-5934.
20. Jeun M, Kim Y J, Park K H, Paek S H, Bae S 2013 Physical contribution of Néel and Brown relaxation to interpreting intracellular hyperthermia characteristics using superparamagneticnanofluids *Journal of nanoscience and nanotechnology* **13** 5719-5725.
21. Kossatz S, Ludwig R, Dähring H, Ettelt V, Rimkus G, Marciello M, Hilger I 2014 High therapeutic efficiency of magnetic hyperthermia in xenograft models achieved with moderate temperature dosages in the tumor area *Pharmaceutical research* **31** 3274-3288.
22. Piñeiro Y, Vargas Z, Rivas J, López‐Quintela M A 2015 Iron Oxide Based Nanoparticles for Magnetic Hyperthermia Strategies in Biological Applications. *European Journal of Inorganic Chemistry* **2015** 4495-4509.
23. Li J, Gong X M, Lin Y Q, Liu X D, Chen L L, Li J M, Li D C 2014 Investigation into loss in ferrofluid magnetization *AIP Advances* **4** 077123.
24. Soukup D, Moise S, Céspedes E, Dobson J, Telling N D 2015 In situ measurement of magnetization relaxation of internalized nanoparticles in live cells *ACS nano* **9** 231-240
25. Sanz B, Calatayud M P, De Biasi E, Lima Jr E, Mansilla M V, Zysler R D, Ibarra M R & Goya G F 2016 In silico before in vivo: how to predict the heating efficiency of magnetic nanoparticles within the intracellular space. *Scientific reports* **6** 38733.
26. Cabrera D, Coene A, Leliaert J, Artés-Ibáñez E J, Dupré L, Telling N D, & Teran F J 2018 Dynamical magnetic response of iron oxide nanoparticles inside live cells. *ACS nano* **12** 2741-2752.
27. Engelmann U, Buhl E M, Baumann M, Schmitz-Rode T & Slabu I Agglomeration of magnetic nanoparticles and its effects on magnetic hyperthermia. *Current Directions in Biomedical Engineering* **3** 457-460.
28. Guardia P, Di Corato R, Lartigue L, Wilhelm C, Espinosa A, Garcia-Hernandez M, Pellegrino T

2012 Water-soluble iron oxide nanocubes with high values of specific absorption rate for cancer cell hyperthermia treatment *ACS nano* **6** 3080-3091.
29. Levy M, Wilhelm C, Luciani N, Deveaux V, Gendron F, Luciani A, Gazeau F 2011 Nanomagnetism reveals the intracellular clustering of iron oxide nanoparticles in the organism *Nanoscale* **3** 4402-4410.
30. Fortin J P, Gazeau F, Wilhelm C 2008 Intracellular heating of living cells through Néel relaxation of magnetic nanoparticles *European Biophysics Journal* **37** 223-228.
31. Lévy M, Wilhelm C, Devaud M, Levitz P, Gazeau F 2012 How cellular processing of superparamagnetic nanoparticles affects their magnetic behavior and NMR relaxivity *Contrast Media & Molecular Imaging* **7** 373-383.
32. Lévy M, Gazeau F, Bacri J C, Wilhelm C, Devaud M 2011 Modeling magnetic nanoparticle dipole-dipole interactions inside living cells *Physical Review B* **84** 075480.
33. Wilhelm C, Gazeau F 2008 Universal cell labelling with anionic magnetic nanoparticles *Biomaterials* **29** 3161-3174.
34. Cabrera D, Camarero J, Ortega D, Teran F J 2015 Influence of the aggregation, concentration, and viscosity on the nanomagnetism of iron oxide nanoparticle colloids for magnetic hyperthermia *Journal of Nanoparticle Research* **17** 1-6.
35. Etheridge M L, Hurley K R, Zhang J, Jeon S, Ring H L, Hogan C, Bischof J C 2014 Accounting for biological aggregation in heating and imaging of magnetic nanoparticles *Technology* **2** 214-228.
36. Fortin J P, Wilhelm C, Servais J, Ménager C, Bacri J C, Gazeau F 2007 Size-sorted anionic iron oxide nanomagnets as colloidal mediators for magnetic hyperthermia. *J.Am.Chem. Soc.* **129** 2628-2635.
37. Tao H, Kaplan D L, Omenetto F G 2012 Silk materials–a road to sustainable high technology *Advanced materials* **24** 2824-2837.
38. Fernández-García L, Marí-Buyé N, Barios J A, Madurga R, Elices M, Pérez-Rigueiro J, González-Nieto D 2016 Safety and tolerability of silk fibroin hydrogels implanted into the mouse brain *Acta biomaterialia* **45** 262-275.
39. Giri S, Trewyn B G, Stellmaker M P, Lin V S Y 2005 Stimuli ‐responsive controlled ‐release delivery system based on mesoporous silica nanorods capped with magnetic nanoparticles *Angewandte Chemie International Edition* **44** 5038-5044.
40. Rockwood D N, Preda R C, Yücel T, Wang X, Lovett M L, Kaplan D L 2011 Materials fabrication from Bombyxmori silk fibroin *Nature protocols* **6** 1612:1631.
41. Hollick E J, Spalton D J, Ursell P G, Pande M V 1998 Biocompatibility of poly (methyl methacrylate), silicone, and AcrySof intraocular lenses: randomized comparison of the cellular reaction on the anterior lens surface *Journal of Cataract & Refractive Surgery* **24** 361-366.
42. Ito Y, Liu S Q, Imanishi Y 1991 Enhancement of cell growth on growth factor-immobilized polymer film *Biomaterials* **12** 449-453.
43. Harrell J W 1999 Effect of AC gradient field on magnetic measurements with an alternating gradient magnetometer *Journal of magnetism and magnetic materials* **205** 121-129.
44. Rohrer M, Bauer H, Mintorovitch J, Requardt M, Weinmann H J 2005 Comparison of magnetic properties of MRI contrast media solutions at different magnetic field strengths *Investigative radiology* **40** 715-724.
45. Laurent S, Forge D, Port M, Roch A, Robic C, Vander Elst L, Muller R N 2008 Magnetic iron oxide nanoparticles: synthesis, stabilization, vectorization, physicochemical characterizations, and biological applications *Chemical reviews* **108** 2064-2110.
46. Poperechny I S, Raikher Y L, Stepanov V I 2010 Dynamic magnetic hysteresis in single-domain particles with uniaxial anisotropy *Physical Review B* **82** 174423.

47. Mehdaoui B, Tan R P, Meffre A, Carrey J, Lachaize S, Chaudret B, Respaud M 2013 Increase of magnetic hyperthermia efficiency due to dipolar interactions in low-anisotropy magnetic nanoparticles: Theoretical and experimental results *Physical Review B* **87** 174419.
48 Yang C, Bian X, Qin J, Zhao X, Zhang K, Bai Y 2014 An investigation of a viscosity-magnetic field hysteretic effect in nano-ferrofluid *Journal of Molecular Liquids* **196** 357-362.
49. Martsenyuk M A, Raikher Y L, Shliomis M I 1974 On the kinetics of magnetization of suspension of ferromagnetic particles *Journal of Experimental and Theoretical Physics* **38** 413-416.
50. Zubarev A Y, Iskakova L Y 2004 To the theory of rheological properties of ferrofluids: influence of drop-like aggregates *Physica A: Statistical Mechanics and its Applications* **343** 65-80.
51. Patel R, Chudasama B 2009 Hydrodynamics of chains in ferrofluid-based magnetorheological ffluids under rotating magnetic field *Physical Review E* **80** 012401.
52. Van Ewijk G A, Vroege G J, Philipse A P 2002 Susceptibility measurements on a fractionated aggregate-free ferrofluid *Journal of Physics: Condensed Matter* **14** 4915
53. Vargas J M, Nunes W C, Socolovsky L M, Knobel M, Zanchet D 2005 Effect of dipolar interaction observed in iron-based nanoparticles *Physical Review B* **72** 184428.
54. Urtizberea A, Natividad E, Arizaga A, Castro M, Mediano A 2010 Specific absorption rates and magnetic properties of ferrofluids with interaction effects at low concentrations *The Journal of Physical Chemistry C* **114** 4916-4922.
55. Serantes D, Baldomir D, Martinez-Boubeta C, Simeonidis K, Angelakeris M, Natividad E, Balcells L I 2010 Influence of dipolar interactions on hyperthermia properties of ferromagnetic particles *Journal of Applied Physics* **108** 073918.
56. Fatin-Rouge N, Tóth E, Meuli R, Bünzli J C G 2004 Enhanced imaging properties of a Gd III complex with unusually large relaxivity *Journal of alloys and compounds* **374** 298-302.
57. Safi M, Sarrouj H, Sandre O, Mignet N, Berret J F 2010 Interactions between sub-10-nm iron and cerium oxide nanoparticles and 3T3 fibroblasts: the role of the coating and aggregation state *Nanotechnology* **21** 145103.
58. Singh N, Manshian B, Jenkins G J, Griffiths S M, Williams P M, Maffeis T G, Doak S H 2009 NanoGenotoxicology: the DNA damaging potential of engineered nanomaterials *Biomaterials* **30** 3891-3914.
59. Brandenberger C, Mühlfeld C, Ali Z, Lenz AG, Schmid O, Parak W J, Rothen‐Rutishauser B 2010 Quantitative Evaluation of Cellular Uptake and Trafficking of Plain and Polyethylene Glycol‐Coated Gold Nanoparticles *Small* **6** 1669-1678.
60. Jonsson T, Nordblad P, Svedlindh P 1998 Dynamic study of dipole-dipole interaction effects in a magnetic nanoparticle system *Physical Review B* **57** 497-504.